

Review of the online analyses of multi-messenger alerts and electromagnetic transient events with the ANTARES neutrino telescope

A. Albert^{1,2} S. Alves³ M. André⁴ M. Ardid⁵ S. Ardid⁵
J.-J. Aubert⁶ J. Aublin⁷ B. Baret⁷ S. Basa⁸ B. Belhorma⁹
M. Bendahman^{7,10} F. Benfenati^{11,12} V. Bertin⁶ S. Biagi¹³
M. Bissinger¹⁴ J. Boumaaza¹⁰ M. Bouta¹⁵ M.C. Bouwhuis¹⁶
H. Brânzaş¹⁷ R. Bruijn^{16,18} J. Brunner⁶ J. Busto⁶ B. Caiffi¹⁹
D. Calvo³ S. Champion^{20,21} A. Capone^{20,21} L. Caramete¹⁷ J. Carr⁶
V. Carretero³ S. Celli^{20,21} M. Chabab²² T. N. Chau⁷
R. Cherkaoui El Moursli¹⁰ T. Chiarusi¹¹ M. Circella²³
J.A.B. Coelho⁷ A. Coleiro⁷ R. Coniglione¹³ P. Coyle⁶
A. Creusot⁷ A. F. Díaz²⁴ B. De Martino⁶ C. Distefano¹³
I. Di Palma^{20,21} A. Domi^{16,18} C. Donzaud^{7,25} D. Dornic⁶
D. Drouhin^{1,2} T. Eberl¹⁴ T. van Eeden¹⁶ D. van Eijk¹⁶
N. El Khayati¹⁰ A. Enzenhöfer⁶ M. Fasano^{20,21} P. Fermani^{20,21}
G. Ferrara¹³ F. Filippini^{11,12} L. Fusco²⁶ S. Gagliardini^{20,21}
J. García⁵ P. Gay^{27,7} N. Geißelbrecht¹⁴ H. Glotin²⁸ R. Gozzini³
R. Gracia Ruiz¹⁴ K. Graf¹⁴ C. Guidi^{19,29} L. Haegel⁷ S. Hallmann¹⁴
H. van Haren³⁰ A.J. Heijboer¹⁶ Y. Hello³¹ J.J. Hernández-Rey³
J. Hößl¹⁴ J. Hofestädt¹⁴ F. Huang⁶ G. Illuminati^{11,12}
C. W. James³² B. Jisse-Jung¹⁶ M. de Jong^{16,33} P. de Jong^{16,18}
M. Kadler³⁴ O. Kalekin¹⁴ U. Katz¹⁴ A. Kouchner⁷
I. Kreykenbohm³⁵ V. Kulikovskiy¹⁹ R. Lahmann¹⁴
M. Lamoureux⁷ D. Lefèvre³⁶ E. Leonora³⁷ G. Levi^{11,12}
S. Le Stum⁶ D. Lopez-Coto³⁸ S. Loucatos^{39,7} L. Maderer⁷
J. Manczak³ M. Marcelin⁸ A. Margiotta^{11,12} A. Marinelli⁴⁰
J.A. Martínez-Mora⁵ K. Melis^{16,18} P. Migliozzi⁴⁰ A. Moussa¹⁵
R. Muller¹⁶ L. Nauta¹⁶ S. Navas³⁸ E. Nezri⁸ B. Ó Fearraigh¹⁶

A. Păun¹⁷ G.E. Păvălaș¹⁷ C. Pellegrino^{11,41,42} M. Perrin-Terrin⁶
V. Pestel¹⁶ P. Piattelli¹³ C. Pieterse³ C. Poirè⁵ V. Popa¹⁷
T. Pradier¹ N. Randazzo³⁷ D. Real³ S. Reck¹⁴ G. Riccobene¹³
A. Romanov^{19,29} A. Saina³ A. Sánchez-Losa^{3,23} F. Salesa Greus³
D. F. E. Samtleben^{16,33} M. Sanguineti^{19,29} P. Sapienza¹³
J. Schnabel¹⁴ J. Schumann¹⁴ F. Schüssler³⁹ J. Seneca¹⁶
M. Spurio^{11,12} Th. Stolarczyk³⁹ M. Taiuti^{19,29} Y. Tayalati¹⁰
S.J. Tingay³² B. Vallage^{29,7} V. Van Elewyck^{7,43} F. Versari^{11,12,7}
S. Viola¹³ D. Vivolo^{40,44} J. Wilms³⁵ S. Zavatarelli¹⁹
A. Zegarelli^{20,21} J.D. Zornoza³ J. Zúñiga³

¹Université de Strasbourg, CNRS, IPHC UMR 7178, F-67000 Strasbourg, France

²Université de Haute Alsace, F-68100 Mulhouse, France

³IFIC - Instituto de Física Corpuscular (CSIC - Universitat de València) c/ Catedrático José Beltrán, 2 E-46980 Paterna, Valencia, Spain

⁴Technical University of Catalonia, Laboratory of Applied Bioacoustics, Rambla Exposició, 08800 Vilanova i la Geltrú, Barcelona, Spain

⁵Institut d'Investigació per a la Gestió Integrada de les Zones Costaneres (IGIC) - Universitat Politècnica de València. C/ Paranimf 1, 46730 Gandia, Spain

⁶Aix Marseille Univ, CNRS/IN2P3, CPPM, Marseille, France

⁷Université Paris Cité, CNRS, Astroparticule et Cosmologie, F-75013 Paris, France

⁸Aix Marseille Univ, CNRS, CNES, LAM, Marseille, France

⁹National Center for Energy Sciences and Nuclear Techniques, B.P.1382, R. P.10001 Rabat, Morocco

¹⁰University Mohammed V in Rabat, Faculty of Sciences, 4 av. Ibn Battouta, B.P. 1014, R.P. 10000 Rabat, Morocco

¹¹INFN - Sezione di Bologna, Viale Berti-Pichat 6/2, 40127 Bologna, Italy

¹²Dipartimento di Fisica e Astronomia dell'Università, Viale Berti Pichat 6/2, 40127 Bologna, Italy

¹³INFN - Laboratori Nazionali del Sud (LNS), Via S. Sofia 62, 95123 Catania, Italy

¹⁴Friedrich-Alexander-Universität Erlangen-Nürnberg, Erlangen Centre for Astroparticle Physics, Erwin-Rommel-Str. 1, 91058 Erlangen, Germany

¹⁵University Mohammed I, Laboratory of Physics of Matter and Radiations, B.P.717, Oujda 6000, Morocco

¹⁶Nikhef, Science Park, Amsterdam, The Netherlands

¹⁷Institute of Space Science, RO-077125 Bucharest, Măgurele, Romania

¹⁸Universiteit van Amsterdam, Instituut voor Hoge-Energie Fysica, Science Park 105, 1098 XG Amsterdam, The Netherlands

¹⁹INFN - Sezione di Genova, Via Dodecaneso 33, 16146 Genova, Italy

²⁰INFN - Sezione di Roma, P.le Aldo Moro 2, 00185 Roma, Italy

²¹Dipartimento di Fisica dell'Università La Sapienza, P.le Aldo Moro 2, 00185 Roma, Italy

²²LPHEA, Faculty of Science - Semlali, Cadi Ayyad University, P.O.B. 2390, Marrakech, Morocco.

²³INFN - Sezione di Bari, Via E. Orabona 4, 70126 Bari, Italy

²⁴Department of Computer Architecture and Technology/CITIC, University of Granada, 18071 Granada, Spain

²⁵Université Paris-Sud, 91405 Orsay Cedex, France

²⁶Università di Salerno e INFN Gruppo Collegato di Salerno, Dipartimento di Fisica, Via Giovanni Paolo II 132, Fisciano, 84084 Italy

- ²⁷Laboratoire de Physique Corpusculaire, Clermont Université, Université Blaise Pascal, CNRS/IN2P3, BP 10448, F-63000 Clermont-Ferrand, France
- ²⁸LIS, UMR Université de Toulon, Aix Marseille Université, CNRS, 83041 Toulon, France
- ²⁹Dipartimento di Fisica dell'Università, Via Dodecaneso 33, 16146 Genova, Italy
- ³⁰Royal Netherlands Institute for Sea Research (NIOZ), Landsdiep 4, 1797 SZ 't Horntje (Texel), the Netherlands
- ³¹Géoazur, UCA, CNRS, IRD, Observatoire de la Côte d'Azur, Sophia Antipolis, France
- ³²International Centre for Radio Astronomy Research - Curtin University, Bentley, WA 6102, Australia
- ³³Huygens-Kamerlingh Onnes Laboratorium, Universiteit Leiden, The Netherlands
- ³⁴Institut für Theoretische Physik und Astrophysik, Universität Würzburg, Emil-Fischer Str. 31, 97074 Würzburg, Germany
- ³⁵Dr. Reimis-Sternwarte and ECAP, Friedrich-Alexander-Universität Erlangen-Nürnberg, Sternwartstr. 7, 96049 Bamberg, Germany
- ³⁶Mediterranean Institute of Oceanography (MIO), Aix-Marseille University, 13288, Marseille, Cedex 9, France; Université du Sud Toulon-Var, CNRS-INSU/IRD UM 110, 83957, La Garde Cedex, France
- ³⁷INFN - Sezione di Catania, Via S. Sofia 64, 95123 Catania, Italy
- ³⁸Dpto. de Física Teórica y del Cosmos & C.A.F.P.E., University of Granada, 18071 Granada, Spain
- ³⁹IRFU, CEA, Université Paris-Saclay, F-91191 Gif-sur-Yvette, France
- ⁴⁰INFN - Sezione di Napoli, Via Cintia 80126 Napoli, Italy
- ⁴¹Museo Storico della Fisica e Centro Studi e Ricerche Enrico Fermi, Piazza del Viminale 1, 00184, Roma
- ⁴²INFN - CNAF, Viale C. Berti Pichat 6/2, 40127, Bologna
- ⁴³Institut Universitaire de France, 75005 Paris, France
- ⁴⁴Dipartimento di Fisica dell'Università Federico II di Napoli, Via Cintia 80126, Napoli, Italy

E-mail: dornic@cppm.in2p3.fr

Abstract. By constantly monitoring a very large portion of the sky, neutrino telescopes are [well-designed](#) to detect neutrinos emitted by transient astrophysical events. Real-time searches with the ANTARES telescope have been performed to look for neutrino candidates coincident with gamma-ray bursts detected by the *Swift* and *Fermi* satellites, high-energy neutrino events registered by IceCube, transient events from blazars monitored by HAWC, photon-neutrino coincidences by AMON notices and gravitational wave candidates observed by LIGO/Virgo. By requiring temporal coincidence, this approach increases the sensitivity and the significance of a potential discovery. This paper summarises the results of the follow-up performed [of](#) the ANTARES telescope between January 2014 and February 2022, which corresponds to the end of the [data-taking](#) period.

Contents

1	Introduction	1
2	Follow-up of IceCube neutrino alerts	3
3	Follow-up of LIGO/Virgo gravitational wave alerts	4
4	Follow-up of gamma-ray bursts	11
5	Follow-up of HAWC alerts for transient phenomena	12
6	Conclusions	13

1 Introduction

Multi-messenger approaches consisting of concomitant searches for the same sources with neutrino telescopes, gravitational wave interferometers and/or multi-wavelength facilities constitute a privileged way of identifying astrophysical cosmic-ray accelerators. Neutrino astronomy allows the study of the most energetic non-thermal processes in the Universe and provides insight into source characteristics not accessible through other messengers. By constantly monitoring at least one complete hemisphere of the sky, neutrino telescopes are well-designed to detect neutrinos emitted by transient phenomena. Real-time searches with the ANTARES telescope have been performed to look for neutrino candidates coincident with gamma-ray bursts detected by the Swift and Fermi satellites, high-energy neutrino events registered by IceCube, transient events from blazars monitored by HAWC, photon-neutrino coincidences by AMON notices and gravitational wave candidates observed by LIGO/Virgo. Requiring a spatial and temporal coincidence with other messengers increases the sensitivity and the significance of a potential discovery with respect to a solely neutrino based search.

The ANTARES telescope, completed in 2008, was the first operating neutrino telescope in the Mediterranean Sea [1]. It was composed of 12 detection lines of about 500 m height anchored at 2475 m depth offshore Toulon (42°48'N, 6°10'E). The mean distance between lines was about 65 m. Each line was made of 25 storeys with an inter-storey distance of 14.5 m. Every storey held three optical modules housing a single 10-inch diameter photomultiplier tube (PMT) looking downward at an angle of 45°. In total, a ~ 10 Mt mass of water was instrumented with 885 optical modules. ANTARES had an average data-taking efficiency larger than 94 % with an effective area decreasing in time due to a loss of optical modules in operation. The data losses can be due to the shutdown of data-taking, calibration periods or too high bioluminescence activities. The ANTARES data acquisition was switched off mid February 2022, when KM3NeT [2] reached a comparable instantaneous sensitivity to cosmic neutrinos.

In the online analysis framework, a dedicated real-time pipeline was developed to look for neutrino events in both temporal and spatial coincidence with transient events announced by public alerts distributed through the Gamma-ray Coordinates Network (GCN [https:](https://)

[//gcn.gsfc.nasa.gov](https://gcn.gsfc.nasa.gov)) or by private alerts transmitted via special channels (i.e. special private requests from external communities). This analysis framework also hosted a neutrino alert sending program [3]. The online selection was optimised to yield a neutrino sample (atmospheric and cosmic) with a minimal contamination from atmospheric muons. Similar cuts as the ones designed for the ANTARES standard offline point-like source search [4] were applied here: only upgoing track events with a good reconstruction quality are used in the analysis to ensure a median angular resolution of about 0.5° . This leads to an atmospheric muon contamination lower than 10 % [5]. The typical rate of neutrino candidates after selection in ANTARES is shown in Figure 1, revealing a slow continuous efficiency loss of the detector [6]. The online analysis used an ideal static detector both for the trigger and the reconstruction. It did not include [knowledge](#) of the dynamical positioning and the precise charge and time calibration sets, which were made available a few months later for the offline analysis.

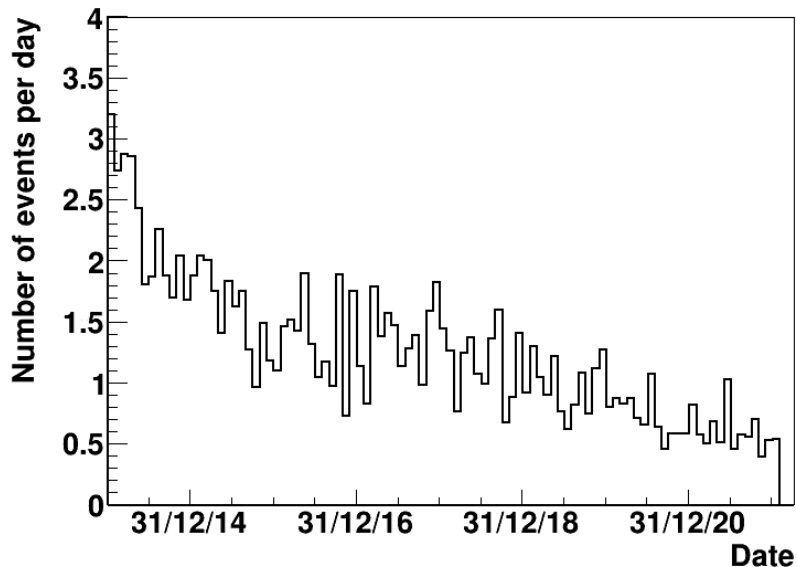


Figure 1. Evolution of the average number of neutrinos per day (averaged during a month period) between 2014 and 2022 selected for the ANTARES online analysis.

For interesting cases, more optimised offline analyses, using the most precise knowledge of the detector, are then performed to improve the online search [7]. Offline searches are also performed for neutrino counterparts to catalogued transients [8, 9].

This paper focuses on the outcomes of the real-time follow-up program of ANTARES, in operation since 2014. Sections 2 and 3 summarise the results for the triggers provided by IceCube and LIGO/Virgo. Sections 4 and 5 present the follow-up of electromagnetic (EM) transients for gamma-ray bursts (GRB) and transient alerts reported by HAWC, respectively. Conclusions and outlooks are drawn in Section 6.

2 Follow-up of IceCube neutrino alerts

A detection of neutrinos by ANTARES and IceCube telescopes within a close temporal window and with compatible directions (coincidence) would be [strong evidence](#) of their astrophysical origin and would point directly to the position of the source in the sky. An alert for a neutrino coincidence would be so rare [that the astronomy community would be motivated to perform a prompt](#) and multi-frequency EM follow-up.

Since 2016, IceCube has been sending public triggers [10] for high-energy starting events (HESE) and extremely high-energy track candidates (EHE). The events are received by the Astrophysical Multi-messenger Observatory Network (AMON [11]) and distributed to the community via an alert of the GCN. In June 2019, IceCube substituted these alerts with two new [very-high-energy](#) track event samples: gold (with a probability to be astrophysical $> 50\%$) and bronze ($> 30\%$) samples [10]. In July 2020, IceCube provided another alert stream based on very high-energy cascades with a typical resolution uncertainty of $15\text{--}20^\circ$ (50% radius) and a typical rate of 8 events per year. The list of triggers is available at this address: <https://gcn.gsfc.nasa.gov/amon.html>.

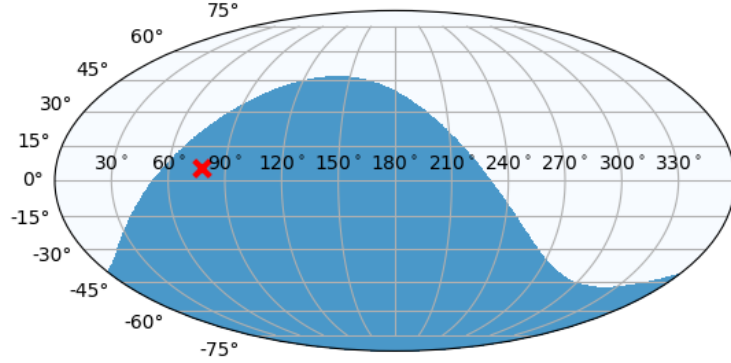


Figure 2. Sky map in equatorial coordinates showing in blue the visible ANTARES field of view at the time of IC170922. The direction of the IC event is drawn as a red cross.

In this context, follow-up analyses have been performed for each IceCube event [with a position on the sky below](#) the horizon of ANTARES (which could consequently yield an upgoing event at the time of the alert). ANTARES has received 115 neutrino triggers from the IceCube alert system and has followed 37 alerts (7 HESE, 3 EHE, 10 gold and 17 bronze). The rest of the triggers was either retracted by the IceCube Collaboration or located in the opposite hemisphere. As an illustration, Figure 2 shows the direction of the IceCube event IC170922 and the ANTARES visibility (i.e., the visible solid angle yielding upgoing events) at the time of the event. No neutrino candidates were found within a cone of 3° centred on the

IceCube event coordinates and a time window of ± 1 hour, further extended to ± 1 day. These non-detections have been used to derive preliminary 90 % confidence level (C.L.) upper limits on the radiant neutrino fluence¹ of the possible sources [producing](#) these events of the order of $\sim 15 \text{ GeV cm}^{-2}$ and $\sim 30 \text{ GeV cm}^{-2}$ for the assumed E^{-2} and the $E^{-2.5}$ differential neutrino fluxes, respectively (see columns 3 and 4 in Table 1). These results have been published as GCN circulars and Astronomer’s Telegrams typically one day after the alerts (columns 5 and 6 in Table 1).

Given the importance of some of the IceCube alerts, dedicated offline analyses have been performed for the following events: IC170922A and the blazar TXS0506+056 [12], [and](#) IC191001A / IC200530A and the tidal disruption events AT2019dsg / AT2019fdr [13]. An off-line time and space correlation analysis for 54 IceCube high-energy track-like neutrino events was performed with the ANTARES neutrino offline data set, resulting in no significant coincidences [14].

3 Follow-up of LIGO/Virgo gravitational wave alerts

Current modeling of the binary black-hole merger evolution does not imply EM or neutrino counterparts. However, in a sufficiently dense circumbinary region, an accretion disk might form and/or a relativistic jet connected to the accretion could be released. Accreting black holes can drive relativistic outflows [15]. In this case, the process might lead to gamma-ray emission with a potential high-energy neutrino counterpart if a hadronic component is present [16–21]. More GW detections will [probe](#) poorly known systems, *i.e.* [those](#) with asymmetric masses, or very large masses, thus leaving room for possible discoveries. An EM counterpart, presumably associated with [hadronic](#) emission is more likely from neutron star/black hole (NSBH) or neutron star/neutron star (BNS) mergers. Most of the models are based either on the formation of a gamma-ray burst [22–24] or a magnetar [25]. The other advantage provided by neutrino follow-up is that the angular resolution of ANTARES [3] ($\sim 0.5^\circ$ at $\sim 10 \text{ TeV}$) compared to the size of the gravitational wave error box (a few hundreds of square degrees on the sky) offers the possibility to drastically reduce the size of the region of interest in case of a coincident neutrino detection.

During the first observing run O1 in 2015, three GW events coming from binary black hole (BBH) mergers were detected by the LIGO interferometers [26]. As the GW online analysis was not ready at that time, only offline analyses have been performed by the ANTARES Collaboration [27, 28]. About one year later, during the second observing run O2 (November 30, 2016 to August 25, 2017), the upgraded LIGO and Virgo detectors observed GWs from seven binary black hole mergers (plus 3 additional sources found in the offline analyses) and the BNS merger GW170817. Only for this last event, EM counterparts have been identified as a short gamma-ray burst followed by a kilonova [7, 29]. During the [O2 run](#), the LIGO/Virgo Collaboration triggered 15 alerts identified by [online](#) analysis using a loose false-alarm-rate threshold of one per month. These triggers were shared with partner collaborations having signed a Memorandum of Understanding with LIGO/Virgo. Each of these alerts were followed by the ANTARES neutrino telescope by searching for a potential neutrino counterpart.

¹The radiant fluence, F , is computed with the formula: $F = \int_{E_{\min}}^{E_{\max}} E \phi_0 \left(\frac{E}{E_0} \right)^{-\gamma} dE$, where ϕ_0 refers to the normalisation of the neutrino spectrum, γ is the spectral index and $E_0 = 1 \text{ GeV}$. $[E_{\min}; E_{\max}]$ corresponds to the 5–95% energy range of the detectable neutrino flux.

The online analysis consists of looking for (i) temporal coincidences within ± 500 seconds and ± 1 hour time windows around the GW alert [30] and (ii) spatial overlap between the 90 % probability contour from GW interferometers and the ANTARES visibility region at the time of the GW event. Figure 3 illustrates the principle of the real-time GW analysis. LIGO and Virgo are sending a few notices for each GW candidate with updated information (Preliminary, Initial, Update, Retraction). Each new type is processed as a new GW trigger. At the end, the results of the last stable revision are provided. This analysis scheme has been applied to all the GW candidate triggers: no upgoing neutrino candidates temporally coincident with any of the GW candidates were found. The results of the nearly real-time analyses have been transmitted to the LIGO/Virgo follow-up community via the GCN. Table 2 lists the different GCN circulars sent on behalf of the ANTARES Collaboration. In general, the online analyses performed for each GW candidate have been followed by a more optimised all-sky analysis [7, 8].

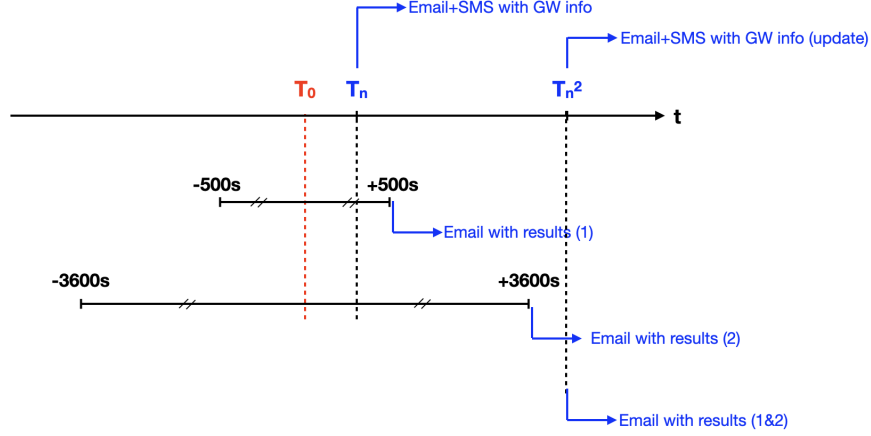


Figure 3. Principle of the online GW analysis. T_0 , T_n and T_{n^2} correspond to the time of the detection, the time of the reception of the first notice and the time of the successive notices for one GW trigger. At the time T_n and when the results of the two searches are available, one email is sent to the ANTARES GW subgroup. An SMS is also sent to speed up communication within the dedicated analysis group.

The third observing run O3 started on April 1st, 2019, with *even-more-upgraded* interferometers. Until the end of March 2020, 78 alerts were distributed publicly, with 22 retracted by LIGO/Virgo after further investigations. Among the 56 events, 37 are classified as BBH, 5 Mass Gap, 4 NSBH, 6 BNS, 1 unmodeled and 3 probably coming from terrestrial noise. The real-time analysis has been performed for 51 GW triggers (Figure 4). Two triggers have not been analysed since the GW were quickly classified as terrestrial noise, 2 had their allowed provenience regions totally outside the ANTARES field of view while for the other events, ANTARES was in maintenance. As an example, Figure 5 illustrates the probability contours of the GW event S190602aq together with the ANTARES visibility at the time of the event. The main characteristics of the 51 GW candidates and the results of the neutrino search are summarised in Table 3.

Figure 6 shows the distribution of the fraction of the 90 % C.L. allowed provenience region visible by the ANTARES detector at the GW detection time, T_0 , as upgoing direc-

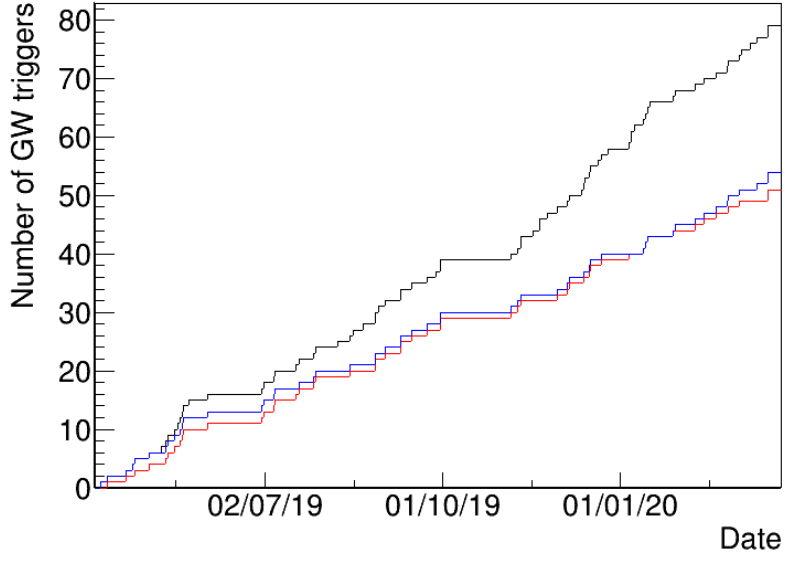


Figure 4. Cumulative number of the GW candidates detected during the O3 run as a function of the date: all GW triggers (black); analysable triggers, i.e., not terrestrial, nor retracted at the time of the analysis (blue); analysed GW candidates (red) by ANTARES.

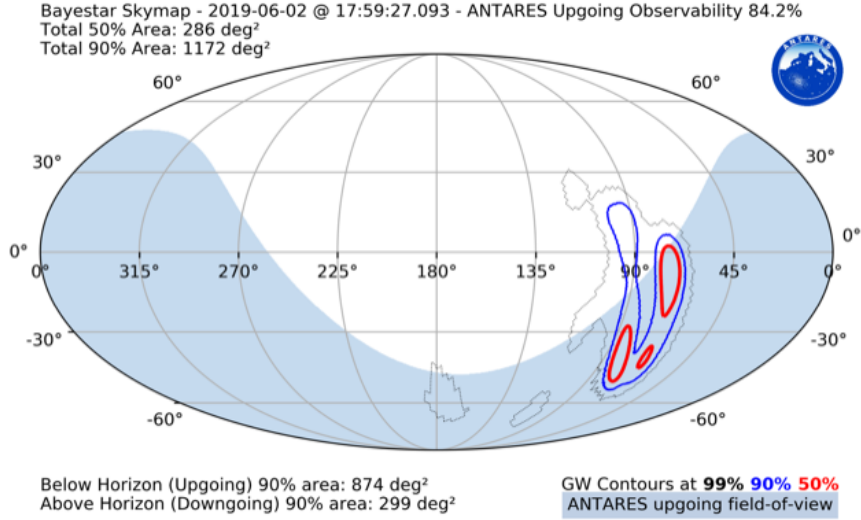


Figure 5. Sky map in equatorial coordinates showing the 99 % (gray), 90 % (blue) and 50 % (red) probability contours for the allowed provenience region of S190602aq together with the ANTARES field of view at the event time (blue part of the map).

tions for all the GW triggers. Unfortunately, during O3, most of the GW candidates were reconstructed with a large allowed provenience region, typically above 1000 deg^2 . Only a few events were reconstructed with a provenience region of less than 100 deg^2 . This makes the EM follow-up even more difficult and the detection of a neutrino more relevant.

For those events detected during the O3 period of GW interferometers, similar analyses to the ones for the O2 events have been performed, but in a completely automated way. No tracks induced by a muon neutrino have been found in time and space coincidence with any alert of run O3 (Table 3). From the non-observation of ANTARES coincidences, upper limits on the neutrino fluence have been estimated (Table 3). All the results have been reported via the publication of a circular to the GCN. The provided information contains a sky map of the visible region of ANTARES (as upgoing) at the time of the GW candidate together with the GW allowed provenience regions (see Figure 5 as an example), the fraction of the GW 90 % allowed provenience region covered by the ANTARES field of view, the number of detected events in time/space coincidence and the expected number of atmospheric background events in the region visible by ANTARES. This expected background rate is computed directly from the data using an off-region area before the GW trigger. The results are reported for two search time windows: ± 500 s and ± 1 hour centred on the time of the GW alert. The typical delay between the detection time of each GW candidate and the time of the ANTARES circular is about 4.5 hours (Figure 7). Note that one necessary condition to submit our results was to receive a confirmation circular by LIGO/Virgo. If this time is used as a reference, the results have been published on average in less than 2 h (Figure 7). The offline analysis has already been done for a few selected events published by LIGO/Virgo [31–33].

Table 3: Characteristics of the GW candidates distributed by LIGO/Virgo during run O3. The coverage indicates the fraction of the 90 % GW allowed provenience region falling in the visibility of ANTARES at the time of the event. The allowed area is the size of the region provided by GW interferometers at the time of the analysis. Some more refined GW parameters may have arrived later. The GW are ordered by date (YYMMDD), contained in the name of the GW (as in GraceDB <https://gracedb.ligo.org/superevents/public/O3/>). The GCN references are the ones published by the ANTARES Collaboration.

GW name	Type	Allowed area (deg ²)	Distance (Mpc)	Coverage (%)	GCN Id
S190412m	BBH	156	812	9.3	24105
S190421ar	BBH	1917	1628	52	24156
S190426c	BNS	1932	377	45	24271
S190503bf	BBH	448	421	98	24387
S190512at	BBH	399	1388	83	24516
S190513bm	BBH	691	1987	55	24539
S190517h	BBH	939	2950	83.3	24581
S190519bj	BBH	967	3154	34	24602
S190521g	BBH	1163	3931	56	24628
S190521r	BBH	388	1136	30	24634
S190602aq	BBH	1172	797	84	24719
S190630ag	BBH	8493	926	68.6	24924
S190701ah	BBH	67	1849	99.9	24952
S190706ai	BBH	1100	5263	48.7	25009

Table 3 – (continued)

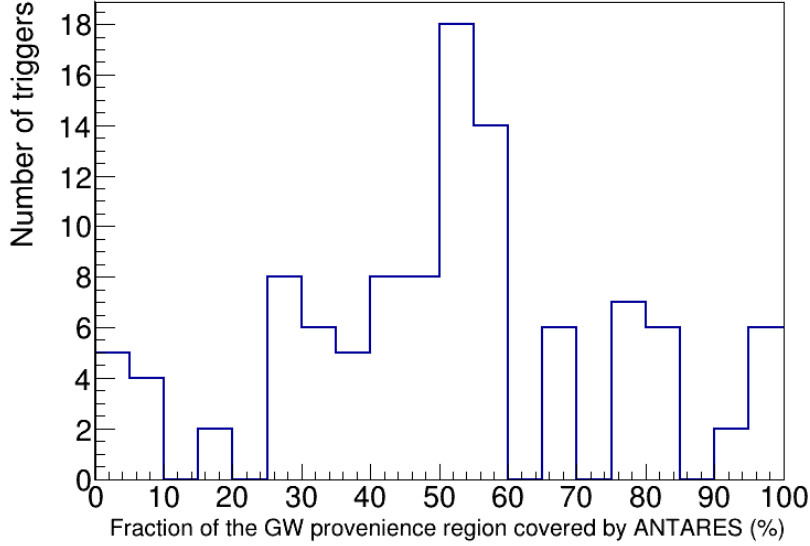
GW name	Type	Allowed area	Distance	Coverage	GCN
S190707q	BBH	1375	874	58.3	25013
S190718y	Terrestrial	7246	227	77.5	25091
S190720a	BBH	1599	869	41.6	25120
S190727h	BBH	1357	2839	55.1	25168
S190728q	BBH	977	874	38.1	25194
S190814bv	NSBH	772	267	99.9	25330
S190828j	BBH	603	1946	53.1	25508
S190828l	BBH	948	1528	56.8	25507
S190901ap	BNS	13613	241	54.1	25611
S190910d	NSBH	3829	632	50.9	25700
S190910h	BNS	24226	230	50	25711
S190915ak	BBH	528	1584	45.6	25758
S190923y	MassGap	2107	438	41.7	25816
S190924h	MassGap	515	514	39.6	25836
S190930s	MassGap	1998	709	25.9	25881
S190930t	NSBH	24220	108	50	25882
S191105e	BBH	1253	1183	66.4	26189
S191109d	BBH	1487	1810	79.1	26210
S191110af	unmodeled	1261		56	26230
S191129u	BBH	1011	742	51.6	26307
S191204r	BBH	433	678	92.9	26336
S191205ah	NSBH	6378	385	28	26352
S191213g	BNS	1393	201	75.1	26404
S191215w	BBH	923	1770	42.3	26443
S191216ap	BBH	300	376	15.9	26458
S191222n	BBH	2324	2518	53.1	26550
S200105ae	Terrestrial	7719	283	35.6	26643
S200112r	BBH	6199	1125	38.4	26718
S200114f	Unmodeled	403		6	26742
S200115j	MassGap	920	340	76	26762
S200128d	BBH	2521	3702	50.1	26912
S200208q	BBH	1120	2142	68.5	27016
S200213t	BNS	2587	201	31.9	27049
S200219ac	BBH	1251	3533	55.5	27135
S200225q	BBH	403	995	42.4	27201
S200302c	BBH	6704	1820	49.5	27284
S200316bj	MassGap	1117	1178	26.6	27390

Table 4: Upper limits (at 90 % C.L.) on neutrino fluence as derived from the non-observation of ANTARES coincidences for the GW candidates distributed by LIGO/Virgo during run O3. The range in the upper limits corresponds to the minimum and maximum values, depending on the local coordinates. For each upper limit, the energy range in which 90 % of events are observed (excluding the 5 % of events with the lower/higher energies) is given. Some more refined GW parameters may have arrived later. The GW are ordered by date (YYMMDD), contained in the name of the GW (as in GraceDB <https://gracedb.ligo.org/superevents/public/O3/>).

GW name	Fluence U.L. (GeV cm ⁻²) at 90 % C.L.	
	$dN/dE \propto E^{-2}$	$dN/dE \propto E^{-2.5}$
S190412m	14 - 16 (3.8 TeV - 3.8 PeV)	38 - 72 (0.6 - 350 TeV)
S190421ar	13 - 21 (2.4 TeV - 1.9 PeV)	28 - 92 (0.5 - 220 TeV)
S190426c	13 - 24 (6.1 TeV - 6.3 PeV)	18 - 60 (1.0 - 560 TeV)
S190503bf	11 - 33 (2.4 TeV - 2.8 PeV)	36 - 145 (0.4 - 240 TeV)
S190512at	15 - 54 (2.5 TeV - 2.9 PeV)	27 - 42 (0.4 - 250 TeV)
S190513bm	15 - 51 (5.1 TeV - 5.4 PeV)	26 - 134 (0.9 - 480 TeV)
S190517h	14 - 111 (2.5 TeV - 2.5 PeV)	32 - 718 (0.4 - 240 TeV)
S190519bj	13 - 185 (4.1 TeV - 4.4 PeV)	22 - 785 (0.7 - 390 TeV)
S190521g	14 - 111 (2.4 TeV - 2.5 PeV)	32 - 943 (0.4 - 230 TeV)
S190521r	14 - 18 (3.0 TeV - 3.1 PeV)	31 - 64 (0.5 - 280 TeV)
S190602aq	13 - 42 (2.6 TeV - 2.9 PeV)	31 - 190 (0.4 - 250 TeV)
S190630ag	13 - 21 (2.7 TeV - 2.9 PeV)	25 - 83 (0.5 - 260 TeV)
S190701ah	15 - 16 (3.1 TeV - 3.2 PeV)	23 - 28 (0.5 - 300 TeV)
S190706ai	12 - 17 (3.7 TeV - 4.0 PeV)	27 - 56 (0.6 - 360 TeV)
S190707q	13 - 34 (3.0 TeV - 3.3 PeV)	20 - 165 (0.5 - 290 TeV)
S190718y	12 - 38 (4.3 TeV - 4.4 PeV)	17 - 2632 (0.7 - 410 TeV)
S190720a	14 - 17 (2.4 TeV - 2.4 PeV)	28 - 83 (0.4 - 230 TeV)
S190727h	14 - 16 (2.4 TeV - 2.1 PeV)	26 - 49 (0.5 - 230 TeV)
S190728q	23 - 24 (4.1 TeV - 4.1 PeV)	86 - 87 (0.6 - 380 TeV)
S190814bv	14 - 20 (2.4 TeV - 2.9 PeV)	51 - 69 (0.4 - 240 TeV)
S190828j	12 - 39 (2.4 TeV - 2.8 PeV)	31 - 190 (0.4 - 240 TeV)
S190828l	14 - 83 (2.4 TeV - 2.7 PeV)	37 - 733 (0.4 - 240 TeV)
S190901ap	12 - 244 (3.3 TeV - 3.4 PeV)	22 - 200 (0.5 - 310 TeV)
S190910d	13 - 54 (2.8 TeV - 2.6 PeV)	20 - 392 (0.5 - 260 TeV)
S190910h	13 - 111 (3.0 TeV - 3.1 PeV)	20 - 562 (0.5 - 290 TeV)
S190915ak	16 - 227 (8.6 TeV - 8.9 PeV)	23 - 366 (0.2 - 750 TeV)
S190923y	13 - 131 (2.9 TeV - 2.7 PeV)	21 - 539 (0.5 - 270 TeV)
S190924h	13 - 16 (3.2 TeV - 3.2 PeV)	46 - 75 (0.5 - 300 TeV)
S190930s	13 - 40 (3.7 TeV - 3.6 PeV)	30 - 172 (0.6 - 340 TeV)
S190930t	13 - 20 (3.2 TeV - 3.3 PeV)	21 - 936 (0.5 - 300 TeV)
S191105e	14 - 18 (2.8 TeV - 3.2 PeV)	24 - 67 (0.5 - 270 TeV)
S191109d	14 - 27 (2.6 TeV - 2.9 PeV)	22 - 72 (0.4 - 250 TeV)

Table 4 – (continued)

GW name	Fluence U.L. E^{-2}	Fluence U.L. $E^{-2.5}$
S191110af	12 - 110 (2.4 TeV - 2.6 PeV)	26 - 94 (0.4 - 240 TeV)
S191129u	13 - 20 (2.7 TeV - 2.4 PeV)	22 - 80 (0.5 - 250 TeV)
S191204r	15 - 16 (2.4 TeV - 2.9 PeV)	26 - 71 (0.4 - 240 TeV)
S191205ah	12 - 297 (3.1 TeV - 3.3 PeV)	24 - 266 (0.5 - 300 TeV)
S191213g	13 - 103 (2.9 TeV - 3.1 PeV)	23 - 733 (0.5 - 280 TeV)
S191215w	14 - 188 (3.3 TeV - 3.3 PeV)	27 - 646 (0.5 - 310 TeV)
S191216ap	13 - 30 (3.1 TeV - 3.2 PeV)	41 - 153 (0.5 - 290 TeV)
S191222n	14 - 42 (2.8 TeV - 2.7 PeV)	22 - 226 (0.5 - 270 TeV)
S200105ae	12 - 100 (3.5 TeV - 3.8 PeV)	22 - 764 (0.6 - 340 TeV)
S200112r	12 - 134 (3.8 TeV - 4.0 PeV)	28 - 770 (0.6 - 360 TeV)
S200114f	12 - 17 (2.4 TeV - 2.9 PeV)	37 - 46 (0.4 - 240 TeV)
S200115j	13 - 136 (3.2 TeV - 3.5 PeV)	24 - 63 (0.5 - 310 TeV)
S200128d	13 - 26 (3.0 TeV - 5.0 PeV)	22 - 127 (0.5 - 290 TeV)
S200208q	19 - 21 (2.4 TeV - 2.9 PeV)	25 - 28 (0.4 - 240 TeV)
S200213t	14 - 121 (5.3 TeV - 5.4 PeV)	15 - 290 (2.0 - 480 TeV)
S200219ac	13 - 82 (3.3 TeV - 3.7 PeV)	24 - 310 (0.6 - 320 TeV)
S200225q	12 - 23 (6.2 TeV - 6.2 PeV)	23 - 62 (1.1 - 570 TeV)
S200302c	12 - 106 (3.5 TeV - 3.8 PeV)	23 - 380 (0.6 - 330 TeV)
S200316bj	13 - 17 (2.4 TeV - 1.9 PeV)	25 - 64 (0.5 - 220 TeV)

**Figure 6.** Distribution of the fraction of the 90 % C.L. allowed provenience region of the GW candidates visible by ANTARES at T_0 as upgoing directions for neutrino candidates..

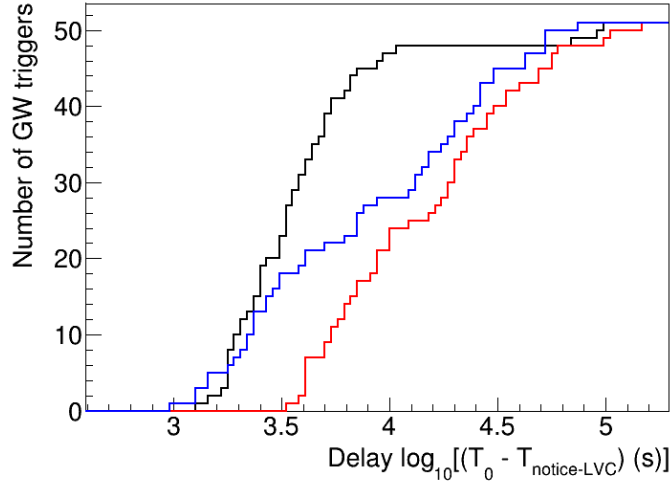


Figure 7. Cumulative distribution of time delays between the time of the 51 GW candidates and the reception time of the first notice (black) and the submission times of the circular with the ANTARES results (red). The blue curve corresponds to the time difference between the reception of the GW confirmation circular and the ANTARES circulars.

4 Follow-up of gamma-ray bursts

Gamma-ray bursts are mainly detected by X-ray and gamma-ray satellites such as *Swift* and *Fermi*. Once a GRB is detected, an alert message is sent publicly via the GCN within a few tens of seconds. Figure 8 left shows the delay of the alert sending for all GRBs detected by Swift and Fermi selected in the ANTARES analysis from 01/2014 to 02/2022 (see below for the details). ANTARES is able to react in real time to this type of alert. Only the bursts with directions below the ANTARES horizon are analysed online. A dedicated search for neutrino-induced muons in the online [data-set](#) is performed in [real-time](#) within a time window $[-250 \text{ s}; +750 \text{ s}]$ around the detection time and in a cone centred on the GRB position. The radius of the cone is determined by taking the maximum between 2° (containing about 90 % of the point spread function, see Figure 3 in Ref. [34]) and the size of the error box provided by Fermi (Figure 8 right). In the case of Swift triggers, a 2° cone is always used. For a cone radius of 2° , the detection of one event yields a p-value (i.e., a probability that the coincidence is due to background) in the range of $2\text{--}5 \times 10^{-5}$. The analysis is performed automatically. To ensure the quality of the data at the alert time, the detector stability is monitored over several hours before the alert, i.e., the reconstructed event rates should follow a Gaussian distribution. This analysis has been operational since the beginning of 2014 and $\sim 98 \%$ of the alerts have been processed. Over more than 8 years of operation (01/2014–02/2022), there were 317 Swift and 770 Fermi-GBM bursts. The bursts detected at the same time by both satellites are tagged with the information provided by Swift. Figure 9 shows the directions of the GRBs of both samples. No online neutrino signals have been detected in this search.

In the case of a coincident neutrino detection (never found in our data), a dedicated offline analysis would have been used to confirm the result and to compute its significance (expected to be higher than 3σ in most of the cases). Using the most precise knowledge of the detector, offline individual and stacked analyses on GRB catalogues have been performed

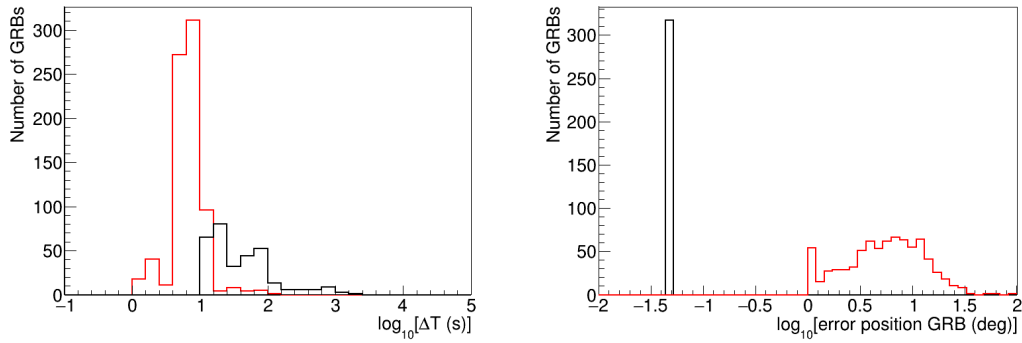


Figure 8. GRBs detected by Swift (black histogram) and Fermi (red histogram) selected in the ANTARES analysis from 01/2014 to 02/2022. (Left) Time delays, ΔT , between the burst detection by Swift and Fermi and the received notice. (Right) Error in the position of the GRBs detected by Swift and Fermi. The information is extracted directly from the GCN notices.

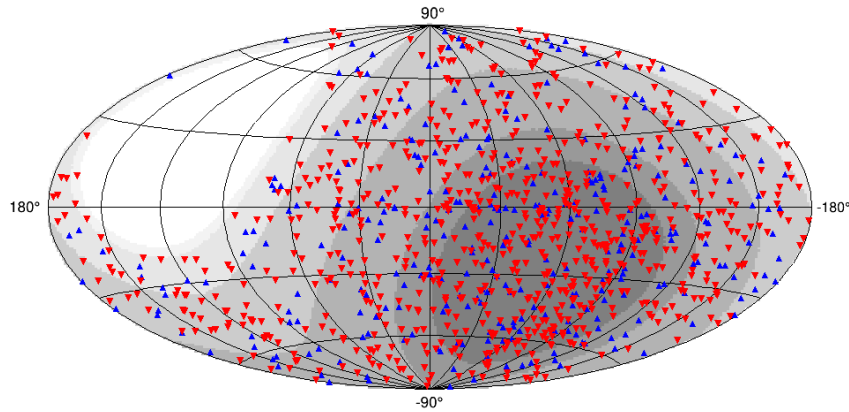


Figure 9. Sky map in Galactic coordinates with the positions of the Fermi (red triangles) and Swift (blue triangles) GRBs followed by ANTARES in the full analysed period (01/2014 to 02/2022). The shade of grey indicates the ANTARES visibility. The darkest region indicates the maximum visibility.

with improved event selections [9, 35, 36].

5 Follow-up of HAWC alerts for transient phenomena

Since mid 2019, the HAWC Collaboration has been issuing alerts of short TeV transients lasting from 0.2 s to 100 s, targeting in particular GRBs. HAWC shares the same advantage as ANTARES, being able to monitor half the sky with a high duty cycle. The quest for TeV gamma rays produced by transient astrophysical sources is particularly interesting for high-energy neutrino telescopes. First, gamma ray detection proves that the sources generating the events are powerful cosmic accelerators. Second, in hadronic production scenarios, these gamma rays have almost the same flux and energy spectrum as the accompanying neutrinos, within the energy range in which the telescope is most sensitive. The alerts are channeled via the AMON framework and then distributed by the GCN. Up to Feb. 2022, the HAWC Collaboration sent 22 triggers, 7 of them with a direction within the ANTARES field of view at

the time of the alert. The alert parameters are available at this address: https://gcn.gsfc.nasa.gov/amon_hawc_events.html. Figure 10 shows the direction of the analysed HAWC alerts together with the integrated ANTARES visibility. The same analysis strategy as for the IceCube neutrino alerts is applied and the results are then published as a circular to the GCN and/or Astronomer’s Telegram. No online neutrinos have been identified in coincidence with the HAWC transients. Table 5 and Table 6 summarise the main alert parameters, the GCN published and the corresponding upper limits for this analysis.

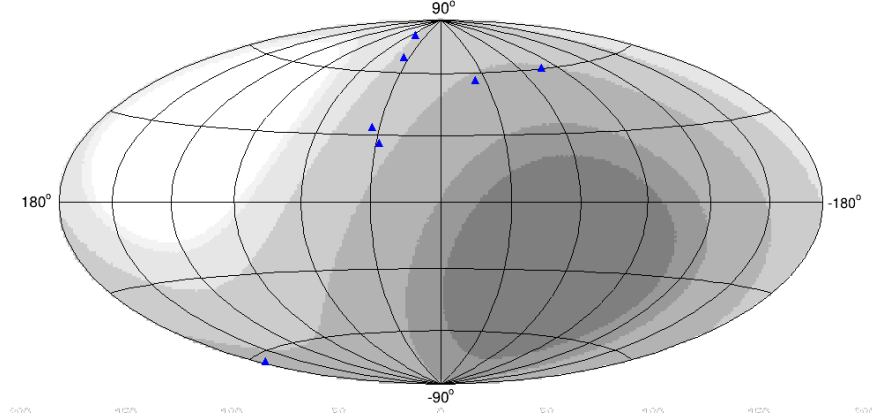


Figure 10. Sky map in Galactic coordinates with the positions of the analysed HAWC alerts (blue triangles) up to Feb 2022. The shade of grey indicates the ANTARES visibility. The darkest region indicates the maximum visibility.

AMON also issues alerts for significant coincidences between ANTARES neutrinos and Fermi/LAT photons and between IceCube neutrinos and HAWC transients. The ANTARES Collaboration has performed a follow-up of the IceCube + HAWC coincidences (NuEM) with a similar analysis method as for the IceCube alerts. The NuEM alert parameters are available at this address: https://gcn.gsfc.nasa.gov/amon_nu_em_coinc_events.html. The event characteristics and the corresponding upper limits are presented in Table 7 and Table 8, together with the reference of the GCN circulars where the results have been published.

6 Conclusions

As a coincident observation by two experiments significantly decreases the probability of false alerts, fast confirmation is essential to allow observatories with limited follow-up capabilities, e.g., due to limited sky coverage or observation time, to efficiently prioritise and schedule their resources. A further advantage is that a subsequent offline analysis of data collected by different instruments upon an alert may yield a statistically relevant result from a combination of signals that by themselves would not be considered significant enough to report.

Public alerts are common for EM transients, especially gamma-ray bursts, soft-gamma repeaters, supernovae, etc. To study the parameters of physical processes inherent to these astrophysical sources, it is necessary to collect as much as possible wide multi-wavelength and multi-probe information as possible. This can only happen with a synergy between different instruments based on efficient, fast and reliable communication between them. The GCN is

in the centre of this strategy as a fast dispatcher of triggers and results. Recently, multi-messenger actors have also adopted a strategy similar to public alert distribution: IceCube in 2016, LIGO/Virgo in 2019, HAWC in 2020. With more than one hundred triggers in one year from the [O3 run](#) of LIGO/Virgo and the new alert selection of IceCube, some maturity has been reached. [A fully automatised online analysis framework has been implemented in the ANTARES Collaboration](#), that looks for time/space coincidences with the time/direction of EM, neutrino and GW transient external triggers. All the received public alerts have been followed provided that at the time of the trigger, their position in the sky was below the horizon for the ANTARES detector. Despite the fact that no coincidences have been found in the online analysis, this effort has highlighted the multi-messenger program of the ANTARES neutrino telescope to a broad community. Most of the remaining work consists in the writing and validation of each GCN circular. This step can also be automatised in the future.

KM3NeT [2] is starting to take data with a sensitivity larger than ANTARES, and this new detector will allow multi-flavor neutrino detection in real time with an unprecedented angular resolution [37]. For the muon-neutrino golden channel, the angular precision can be as low as 0.1° at very high energies. In KM3NeT, all-flavor neutrino events will be used for online follow-up studies in a large energy range from a few GeV to a few PeV.

Acknowledgments

The authors acknowledge the financial support of the funding agencies: Centre National de la Recherche Scientifique (CNRS), Commissariat à l'énergie atomique et aux énergies alternatives (CEA), Commission Européenne (FEDER fund and Marie Curie Program), LabEx UnivEarthS (ANR-10-LABX-0023 and ANR-18-IDEX-0001), Région Alsace (contrat CPER), Région Provence-Alpes-Côte d'Azur, Département du Var and Ville de La Seyne-sur-Mer, France; Bundesministerium für Bildung und Forschung (BMBF), Germany; Istituto Nazionale di Fisica Nucleare (INFN), Italy; Nederlandse organisatie voor Wetenschappelijk Onderzoek (NWO), the Netherlands; Executive Unit for Financing Higher Education, Research, Development and Innovation (UEFISCDI), Romania; Ministerio de Ciencia e Innovación: Programa Estatal para Impulsar la Investigación Científico-Técnica y su Transferencia (refs. PID2021-124591NB-C41, -C42, -C43) (MCIU/FEDER), Programa de Planes Complementarios I+D+I (refs. ASFAE/2022/023, ASFAE/2022/014) and Programa María Zambrano (Spanish Ministry of Universities, funded by the European Union, NextGenerationEU), Generalitat Valenciana: Prometeo (PROMETEO/2020/019), and GenT (refs. CIDEAGENT/2018/034, /2019/043, /2020/049. /2021/23) programs, Junta de Andalucía (ref. SOMM17/6104/UGR, P18-FR-5057), EU: MSC program (ref. 101025085), Spain; Ministry of Higher Education, Scientific Research and Innovation, Morocco, and the Arab Fund for Economic and Social Development, Kuwait. We also acknowledge the technical support of Ifremer, AIM and Foselev Marine for the sea operation and the CC-IN2P3 for the computing facilities.

References

- [1] M. Ageron *et al.*, “ANTARES: the first undersea neutrino telescope,” *Nucl. Instrum. Meth. A*, vol. 656, pp. 11–38, 2011.

- [2] S. Adrian-Martinez *et al.*, “Letter of intent for KM3NeT 2.0,” *J. Phys. G*, vol. 43, no. 8, p. 084001, 2016.
- [3] S. Adrián-Martínez *et al.*, “Optical and X-ray early follow-up of ANTARES neutrino alerts,” *JCAP*, vol. 02, p. 062, 2016.
- [4] A. Albert *et al.*, “ANTARES Search for Point Sources of Neutrinos Using Astrophysical Catalogs: A Likelihood Analysis,” *Astrophys. J.*, vol. 911, no. 1, p. 48, 2021.
- [5] M. Ageron *et al.*, “The ANTARES Telescope Neutrino Alert System,” *Astropart. Phys.*, vol. 35, pp. 530–536, 2012.
- [6] A. Albert *et al.*, “Long-term monitoring of the ANTARES optical module efficiencies using ^{40}K decays in sea water,” *Eur. Phys. J. C*, vol. 78, no. 8, p. 669, 2018.
- [7] A. Albert *et al.*, “Search for High-energy Neutrinos from Binary Neutron Star Merger GW170817 with ANTARES, IceCube, and the Pierre Auger Observatory,” *Astrophys. J. Lett.*, vol. 850, no. 2, p. L35, 2017.
- [8] A. Albert *et al.*, “Search for neutrino counterparts of gravitational-wave events detected by LIGO and Virgo during run O2 with the ANTARES telescope,” *Eur. Phys. J. C*, vol. 80, no. 5, p. 487, 2020.
- [9] S. Adrián-Martínez *et al.*, “Stacked search for time shifted high energy neutrinos from gamma ray bursts with the ANTARES neutrino telescope,” *Eur. Phys. J. C*, vol. 77, no. 1, p. 20, 2017.
- [10] R. Abbasi *et al.*, “Follow-up of Astrophysical Transients in Real Time with the IceCube Neutrino Observatory,” *Astrophys. J.*, vol. 910, no. 1, p. 4, 2021.
- [11] M. Smith *et al.*, “The Astrophysical Multimessenger Observatory Network (AMON),” *Astropart. Phys.*, vol. 45, pp. 56–70, 2013.
- [12] A. Albert *et al.*, “The Search for Neutrinos from TXS 0506+056 with the ANTARES Telescope,” *Astrophys. J. Lett.*, vol. 863, no. 2, p. L30, 2018.
- [13] A. Albert *et al.*, “Search for Neutrinos from the Tidal Disruption Events AT2019dsg and AT2019fdr with the ANTARES Telescope,” *Astrophys. J.*, vol. 920, no. 1, p. 50, 2021.
- [14] A. Albert *et al.*, “ANTARES neutrino search for time and space correlations with IceCube high-energy neutrino events,” *Astrophys. J.*, vol. 879, no. 2, p. 108, 2019.
- [15] P. Meszaros, “Gamma-Ray Bursts,” *Rept. Prog. Phys.*, vol. 69, pp. 2259–2322, 2006.
- [16] R. Moharana, S. Razzaque, N. Gupta, and P. Meszaros, “High Energy Neutrinos from the Gravitational Wave event GW150914 possibly associated with a short Gamma-Ray Burst,” *Phys. Rev. D*, vol. 93, no. 12, p. 123011, 2016.
- [17] K. Kotera and J. Silk, “Ultrahigh Energy Cosmic Rays and Black Hole Mergers,” *Astrophys. J. Lett.*, vol. 823, no. 2, p. L29, 2016.
- [18] R. Perna, D. Lazzati, and B. Giacomazzo, “Short Gamma-Ray Bursts from the Merger of Two Black Holes,” *Astrophys. J. Lett.*, vol. 821, no. 1, p. L18, 2016.
- [19] I. Bartos, B. Kocsis, Z. Haiman, and S. Márka, “Rapid and Bright Stellar-mass Binary Black Hole Mergers in Active Galactic Nuclei,” *Astrophys. J.*, vol. 835, no. 2, p. 165, 2017.
- [20] N. C. Stone, B. D. Metzger, and Z. Haiman, “Assisted inspirals of stellar mass black holes embedded in AGN discs: solving the ‘final au problem’,” *Mon. Not. Roy. Astron. Soc.*, vol. 464, no. 1, pp. 946–954, 2017.
- [21] K. Murase, K. Kashiyama, P. Mészáros, I. Shoemaker, and N. Senno, “Ultrafast Outflows from Black Hole Mergers with a Minidisk,” *Astrophys. J. Lett.*, vol. 822, no. 1, p. L9, 2016.

- [22] S. S. Kimura, K. Murase, I. Bartos, K. Ioka, I. S. Heng, and P. Mészáros, “Transejecta high-energy neutrino emission from binary neutron star mergers,” *Phys. Rev. D*, vol. 98, no. 4, p. 043020, 2018.
- [23] S. S. Kimura, K. Murase, P. Mészáros, and K. Kiuchi, “High-Energy Neutrino Emission from Short Gamma-Ray Bursts: Prospects for Coincident Detection with Gravitational Waves,” *Astrophys. J. Lett.*, vol. 848, no. 1, p. L4, 2017.
- [24] S. S. Kimura, “High-energy emissions from neutron star mergers,” *EPJ Web Conf.*, vol. 210, p. 03001, 2019.
- [25] K. Fang and B. D. Metzger, “High-Energy Neutrinos from Millisecond Magnetars formed from the Merger of Binary Neutron Stars,” *Astrophys. J.*, vol. 849, no. 2, p. 153, 2017.
- [26] B. Abbott *et al.*, “Observation of Gravitational Waves from a Binary Black Hole Merger,” *Phys. Rev. Lett.*, vol. 116, no. 6, p. 061102, 2016.
- [27] S. Adrian-Martinez *et al.*, “High-energy Neutrino follow-up search of Gravitational Wave Event GW150914 with ANTARES and IceCube,” *Phys. Rev. D*, vol. 93, no. 12, p. 122010, 2016.
- [28] A. Albert *et al.*, “Search for High-energy Neutrinos from Gravitational Wave Event GW151226 and Candidate LVT151012 with ANTARES and IceCube,” *Phys. Rev. D*, vol. 96, no. 2, p. 022005, 2017.
- [29] B. Abbott *et al.*, “Multi-messenger Observations of a Binary Neutron Star Merger,” *Astrophys. J. Lett.*, vol. 848, no. 2, p. L12, 2017.
- [30] B. Baret *et al.*, “Bounding the Time Delay between High-energy Neutrinos and Gravitational-wave Transients from Gamma-ray Bursts,” *Astropart. Phys.*, vol. 35, pp. 1–7, 2011.
- [31] B. Abbott *et al.*, “GW190425: Observation of a Compact Binary Coalescence with Total Mass $\sim 3.4 M_{\odot}$,” *Astrophys. J. Lett.*, vol. 892, p. L3, 2020.
- [32] R. Abbott *et al.*, “GW190412: Observation of a Binary-Black-Hole Coalescence with Asymmetric Masses,” *Phys. Rev. D*, vol. 102, no. 4, p. 043015, 2020.
- [33] M. Colomer Molla, B. Baret, A. Coleiro, D. Dornic, and T. Pradier, “Search for neutrino counterparts of cataloged gravitational-wave events detected by Advanced-LIGO and Virgo during run O2 with ANTARES,” *PoS*, vol. ICRC2019, p. 856, 2020.
- [34] A. Albert *et al.*, “First all-flavor neutrino pointlike source search with the ANTARES neutrino telescope,” *Phys. Rev. D*, vol. 96, no. 8, p. 082001, 2017.
- [35] A. Albert *et al.*, “The search for high-energy neutrinos coincident with fast radio bursts with the ANTARES neutrino telescope,” *Mon. Not. Roy. Astron. Soc.*, vol. 482, no. 1, pp. 184–193, 2019.
- [36] A. Albert *et al.*, “Constraining the contribution of Gamma-Ray Bursts to the high-energy diffuse neutrino flux with 10 yr of ANTARES data,” *Mon. Not. Roy. Astron. Soc.*, vol. 500, no. 4, pp. 5614–5628, 2020.
- [37] W. Assal, D. Dornic, F. Huang, E. Le Guirriec, M. Lincetto, and G. Vannoye, “Real-time multi-messenger analysis framework for KM3NeT,” *JINST*, vol. 16, no. 09, p. C09034, 2021.

IceCube event	Elevation	Fluence U.L. (GeV cm ⁻²) at 90 % C.L.		GCN Id	ATels Id
		$dN/dE \propto E^{-2}$	$dN/dE \propto E^{-2.5}$		
IC160731A (EHE/HESE)	-28°	14 (2.8 TeV - 3.1 PeV)	27 (0.4 - 280 TeV)	/	9324
IC160814A (HESE)	-26°	16 (2.9 TeV - 3.3 PeV)	43 (0.5 - 250 TeV)	19885	9440
IC161103A (HESE)	-26°	13 (3.8 TeV - 3.8 PeV)	22 (0.7 - 370 TeV)	20134	9715
IC170321A (EHE)	-57°	16 (2.5 TeV - 2.5 PeV)	26 (0.5 - 220 TeV)	20926	10189
IC170922A (EHE)	-14°	15 (3.3 TeV - 3.4 PeV)	34 (0.5 - 280 TeV)	21923	10773
IC171015A (HESE)	-45°	14 (2.7 TeV - 2.9 PeV)	27 (0.4 - 240 TeV)	22019	10854
IC180908A (EHE)	-41°	18 (2.4 TeV - 2.6 PeV)	36 (0.4 - 250 TeV)	23218	12024
IC190104A (HESE)	-39°	16 (3.2 TeV - 3.5 PeV)	30 (0.6 - 320 TeV)	23611	12359
IC190124A (HESE)	-44°	15 (3.1 TeV - 3.6 PeV)	25 (0.6 - 320 TeV)	23793	12423
IC190504A (HESE)	-18°	16 (3.1 TeV - 3.5 PeV)	32 (0.6 - 320 TeV)	24400	12731
IC190619A (gold)	-19°	13 (3.9 TeV - 3.9 PeV)	33 (0.7 - 320 TeV)	24866	12878
IC190712A (bronze)	-13°	16 (4.6 TeV - 4.3 PeV)	40 (0.8 - 420 TeV)	25064	12937
IC191119A (gold)	-37°	16 (3.4 TeV - 3.6 PeV)	28 (0.7 - 340 TeV)	26266	13295
IC191231A (bronze)	-17°	15 (5.3 TeV - 5.0 PeV)	32 (1.0 - 470 TeV)	26623	13380
IC200127A (bronze)	-18°	15 (6.8 TeV - 6.3 PeV)	29 (1.0 - 610 TeV)	26811	13409
IC200421A (bronze)	-25°	15 (3.9 TeV - 4.9 PeV)	27 (0.7 - 380 TeV)	27619	13654
IC200530A (gold)	-0.04°	80 (6.0 TeV - 6.0 PeV)	110 (1 - 560 TeV)	27871	13770
IC200620A (bronze)	-32°	15 (5.0 TeV - 4.0 PeV)	30 (0.8 - 400 TeV)	28002	13820
IC200911A (bronze)	-7°	14 (10.0 TeV - 8.0 PeV)	34 (1.5 - 740 TeV)	28415	14008
IC200916A (bronze)	-29°	18 (4.0 TeV - 4.5 PeV)	33 (1 - 430 TeV)	28446	14025
IC200926B (bronze)	-13°	15 (8.0 TeV - 7.0 PeV)	35 (1 - 690 TeV)	28515	14045
IC200929A (gold)	-10°	13 (3.0 TeV - 4.0 PeV)	45 (0.7 - 340 TeV)	28535	14054
IC201014A (bronze)	-30°	18 (5.0 TeV - 4.5 PeV)	30 (0.8 - 430 TeV)	28624	14095
IC201021A (bronze)	-14°	19 (5.0 TeV - 5.0 PeV)	48 (0.8 - 430 TeV)	28738	14110
IC201114A (bronze)	-41°	19 (4.0 TeV - 4.0 PeV)	31 (0.7 - 370 TeV)	28890	14176
IC201115A (gold)	-7°	17 (3.2 TeV - 3.2 PeV)	68 (0.6 - 330 TeV)	28901	14181
IC201209A (gold)	-34°	16 (3.0 TeV - 3.0 PeV)	30 (0.5 - 280 TeV)	29023	14259
IC210210A (gold)	-18°	16 (3.5 TeV - 3.7 PeV)	40 (0.7 - 360 TeV)	29475	/
IC210922A (gold)	-37°	16 (3.0 TeV - 3.3 PeV)	30 (0.6 - 300 TeV)	30875	14935
IC210926A (cascade)	-71°	21 (2.3 TeV - 3.2 PeV)	30 (0.4 - 240 TeV)	30887	14938
IC211023A (bronze)	+0.8°	12 (3.0 TeV - 3.0 PeV)	48 (0.6 - 300 TeV)	30971	14995
IC211116A (bronze)	-47°	16 (3.0 TeV - 3.5 PeV)	26 (0.7 - 320 TeV)	31090	15042
IC211117A (gold)	-12°	15 (3.0 TeV - 3.5 PeV)	43 (0.6 - 320 TeV)	31094	15044
IC211125A (bronze)	-6°	12 (5.0 TeV - 5.0 PeV)	35 (1 - 500 TeV)	31128	15065
IC211208A (bronze)	-10°	17 (5.0 TeV - 5.0 PeV)	43 (1 - 500 TeV)	31225	15106
IC211216A (bronze)	-8°	16 (5.0 TeV - 5.0 PeV)	49 (1 - 450 TeV)	31252	15121
IC211216B (bronze)	-4°	17 (5.0 TeV - 5.0 PeV)	40 (1 - 450 TeV)	31262	15127
IC220205B (gold)	-51°	16 (3.0 TeV - 3.3 PeV)	30 (0.6 - 300 TeV)	31556	15207

Table 1. Upper limits (at 90% C.L.) on neutrino fluence as derived from the non-observation of ANTARES coincidences for each IceCube neutrino candidate. For each upper limit, the energy range in which 90% of events are observed (excluding the 5% of events with the lower/higher energies) is given. The publication reference number (Id) in GCN and in Astronomer’s Telegram of the ANTARES follow-up of IceCube public triggers are given in the last two columns.

GW alert	Confirmed GW name	Type	Fluence U.L. E^{-2}	Fluence U.L. $E^{-2.5}$	GCN Id
G268556	GW170104	BBH	12 - 122 (3.6 TeV - 3.9 PeV)	20 - 756 (0.6 - 350 TeV)	20517
G270580		BBH	13 - 48 (4.0 TeV - 4.0 PeV)	19 - 193 (0.7 - 370 TeV)	20621
G274296		BBH	13 - 20 (2.8 TeV - 2.7 PeV)	25 - 79 (0.5 - 270 TeV)	20704
G275404		BBH	14 - 49 (4.1 TeV - 4.4 PeV)	19 - 174 (0.7 - 390 TeV)	20751
G275697		BBH	12 - 25 (3.3 TeV - 3.7 PeV)	22 - 60 (0.5 - 330 TeV)	20765
G277583		BBH	13 - 100 (3.3 TeV - 3.5 PeV)	22 - 477 (0.6 - 310 TeV)	20866
G284239		BBH	13 - 84 (3.2 TeV - 3.4 PeV)	22 - 448 (0.5 - 310 TeV)	21066
G288732	GW170608	BBH	14 - 17 (5.4 TeV - 5.4 PeV)	20 - 53 (0.9 - 490 TeV)	21223
G296853	GW170809	BBH	14 - 17 (2.4 TeV - 2.8 PeV)	35 - 66 (0.4 - 240 TeV)	21433
G297595	GW170814	BBH	13 - 16 (2.4 TeV - 2.8 PeV)	33 - 64 (0.4 - 240 TeV)	21479
G298048	GW170817	BNS			21522 / 21631
G298936	GW170823	BBH	12 - 21 (3.0 TeV - 3.5 PeV)	21 - 68 (0.5 - 300 TeV)	21659
G299232		BBH	15 - 24 (4.3 TeV - 4.5 PeV)	19 - 85 (0.7 - 400 TeV)	21696 / 21769

Table 2. ANTARES analysis results of the GW candidates distributed by LIGO/Virgo during O2 run. Columns 3 and 4 provide the upper limits (at 90 % C.L.) on neutrino fluence as derived from the non-observation of ANTARES coincidences in the upgoing sky for the GW candidates distributed by LIGO/Virgo during run O3 assuming a neutrino energy spectrum of E^{-2} and $E^{-2.5}$. The range in the upper limits corresponds to the minimum and maximum values, depending on the local coordinates. Note that for the event G298048, all the GW provenience area is in the downgoing sky. For each upper limit, the energy range in which 90 % of events are observed (excluding the 5 % of events with the lower/higher energies) is given. The last column gives the references of the GCN circular published by the ANTARES collaboration for each GW candidates.

Event Id	Direction RA, Dec (deg)	Error (arcmin)	δT (s)	Visibility (%)	GCN Id
HAWC-211123A (110400_42)	34.12, -8.04	36	1	53	31111
HAWC-210507A (1010067_1345)	257.24, $+8.09$	24	10	45	29967
HAWC-201019A (1009678_72)	203.15, $+29.70$	36	100	32	28729
HAWC-200709A (1009500_793)	252.38, $+15.20$	24	100	42	28074
HAWC-200226A (19170_50)	182.80, -0.61	48	1	50	27242
HAWC-191210A (9066_1171)	210.80, -1.52	48	0.2	35	26391
HAWC-191019A (8991_1097)	217.50, $+25.81$	48	0.2	50	26049

Table 5. Summary of HAWC transient triggers and ANTARES publication in GCN. "Error" refers to the location uncertainty (radius, 50 % containment). δT is the trigger duration interval. "Visibility" refers to the ANTARES visibility fraction of the alert direction during one day. The last column gives the GCN circular references of the ANTARES follow-up.

Alert	Fluence U.L. (GeV cm^{-2}) at 90 % C.L.	
	$dN/dE \propto E^{-2}$	$dN/dE \propto E^{-2.5}$
HAWC-211123A	17 (3 TeV - 3 PeV)	70 (0.5 - 280 TeV)
HAWC-210507A	15 (4 TeV - 4 PeV)	37 (0.7 - 380 TeV)
HAWC-201019A	17 (7 TeV - 6 PeV)	37 (1 - 630 TeV)
HAWC-200709A	40 (5 TeV - 5 PeV)	240 (0.9 - 430 TeV)
HAWC-200226A	16 (3.2 TeV - 3.4 PeV)	27 (0.6 - 320 TeV)
HAWC-191210A	17 (3 TeV - 3 PeV)	69 (0.6 - 300 TeV)
HAWC-191019A	90 (6 TeV - 6 PeV)	110 (1 - 550 TeV)

Table 6. Upper limits (at 90 % C.L.) on neutrino fluence as derived from the non-observation of ANTARES coincidences for each HAWC transient triggers. For each upper limit, the energy range in which 90 % of events are observed (excluding the 5 % of events with the lower/higher energies) is given.

Alert	Trigger Id	RA,Dec (deg)	R_{err} (deg)	Duration (sec)	Visibility (%)	GCN Id
NuEM-220116A	0_105322	322.13, +27.26	0.17	23130.4	34	31476
NuEM-211209A	0_101674	12.03, -5.75	0.18	18273.3	53	31198
NuEM-211020A	0_96720	99.76, +9.07	0.17	21670.1	45	30954
NuEM-210515B	0_85791	93.93, +12.51	0.2	22165.2	42	30024
NuEM-210515A	0_85790	93.64, +14.66	0.15	22443	42	30024
NuEM-210111A	0_73310	162.34, -19.46	0.37	22742.5	39	29294
NuEM-201124A	0_68186	135.0, +7.74	0.23	21531.2	46	28953
NuEM-201107A	0_66291	140.2, +29.76	0.15	23105.4	30	/
NuEM-200717A	0_54519	118.5, -1.62	0.38	19395.5	50	28144

Table 7. Summary of the ANTARES follow-up of the NuEM triggers (IceCube / HAWC coincidence). R_{err} is the 50 % allowed region. "Duration" corresponds to the duration of the coincidence. The last column gives the GCN circular references of the ANTARES follow-up.

Alert	Fluence U.L. (GeV cm^{-2}) at 90 % C.L.	
	$dN/dE \propto E^{-2}$	$dN/dE \propto E^{-2.5}$
NuEM-220116A	14 (6 TeV - 6 PeV)	31 (1 - 580 TeV)
NuEM-211209A	15 (3 TeV - 3.3 PeV)	26 (0.5 - 290 TeV)
NuEM-211020A	15 (4 TeV - 4 PeV)	26 (0.75 - 380 TeV)
NuEM-210515B	15 (5 TeV - 4 PeV)	30 (1 - 400 TeV)
NuEM-210515A	15 (5 TeV - 4 PeV)	30 (1 - 400 TeV)
NuEM-210111A	14 (5 TeV - 5 PeV)	35 (1 - 480 TeV)
NuEM-201124A	19 (4 TeV - 4 PeV)	31 (0.72 - 380 TeV)
NuEM-200717A	15 (3 TeV - 3.4 PeV)	25 (0.6 - 310 TeV)

Table 8. Upper limits (at 90 % C.L.) on neutrino fluence as derived from the non-observation of ANTARES coincidences for each NuEM triggers. For each upper limit, the energy range in which 90 % of events are observed (excluding the 5 % of events with the lower/higher energies) is given.